Separation and Purification Technology 219 (2019) 208–215

Contents lists available at ScienceDirect

Separation and Purification Technology

journal homepage: www.elsevier.com/locate/seppur

Colloidal deposition on polymer-brush-coated NF membranes

Naama Segev-Mark[a], Anh Vu[b], Ningyuan Chen[a], Xianghong Qian[c], S. Ranil Wickramasinghe[b], Guy Z. Ramon[a,*]

[a] Department of Civil & Environmental Engineering, Technion – Israel Institute of Technology, Haifa 32000, Israel
[b] Ralph E Martin Department of Chemical Engineering, University of Arkansas, Fayetteville, AR 72701, United States
[c] Department of Biomedical Engineering, University of Arkansas, Fayetteville, AR 72701, United States

ARTICLE INFO

Keywords:
Fouling
Surface modifications
Direct microscopic observation

ABSTRACT

Fouling control remains a challenge in membrane separation. Here, nanofiltration (NF) membranes have been modified with poly-N-iso-propylacrylamide (PNIPAM) brushes, fabricated using surface-initiated atom transfer radical polymerization (ATRP). PNIPAM, a thermo-responsive polymer, exhibits a phase transition at its lower critical solution temperature (LCST) of ~32 °C in DI water, which reduces to ~20 °C at high-ionic strength. Direct microscopic observation was employed to investigate, in-situ, the deposition and release patterns and kinetics of colloidal fouling on NF membranes with and without a PNIPAM brush layer. Membrane surfaces were characterized by atomic force microscopy (AFM), X-ray Photoelectron Spectroscopy (XPS), and attenuated total reflection–Fourier transform infrared (ATR-FTIR) analysis. Changes in surface chemistry and morphology confirmed the grafting of PNIPAM with a rougher surface morphology. The permeate flux of grafted membranes with DI water at ~20 °C and ~40 °C indicate reversible conformational changes of PNIPAM. Cross-flow experiments revealed that even though the surface hydrophobicity of the PNIPAM-grafted membranes increased, the brush-coated membrane surfaces hinder particle deposition regardless of particle surface charge, exhibiting considerably lower deposition, compared to the unmodified membrane. Deposition was lower, for both membranes, in the case of negatively charged particles. When the particles had a small positive charge, a significant increase in deposition was observed for the unmodified membrane, compared with the modified membrane, presumably due to the former's larger negative charge. However, particles, once deposited, could generally not be removed by physical rinsing, nor – in the case of the PNIPAM-coated membranes – by switching polymer conformation. Nevertheless, the results of the direct observation can provide valuable insight for further improving fouling-resistant membranes based on polymer brush coatings.

1. Introduction

Fouling affects all membrane-based separation processes. The deposition of colloids, salts, organic matter and the growth of biofilms results in increased energy consumption and compromised permeate quality [1–4]. Colloidal fouling is an important reason for flux decline during nanofiltration (NF) and reverse osmosis (RO). Therefore, membrane cleaning as well as the development of fouling-resistant surfaces is of tremendous practical importance [1,5–7]. Since membrane surface properties strongly affect the adsorption of foulant species, surface modification of the membrane in order to create a fouling-resistant layer has become an attractive method to suppress fouling [2,8–13]. Surface modification aims to improve the anti-fouling properties of the membrane surface while maintaining the desired properties of the barrier layer and support structure.

Previous studies suggest that grafting thermo-responsive polymers like PNIPAM can lead to active release of adsorbed foulants by reversibly switching the conformation of the grafted polymer chains between their hydrated and dehydrated state [12,14,15]. Yu et al. used click chemistry to graft polyzwitterions (PZs) onto polyamide, with anti-fouling properties of the modified membrane assessed by measuring water flux after a cleaning protocol [16]. Liu et al. modified thin-film composite (TFC) membranes with 3D hyperbranched polyglycerol to increase hydrophilicity (water permeability) and membrane fouling resistance of forward osmosis membranes. In this study the anti-fouling properties of the modified membranes were evaluated using static experiments by imaging the adsorbed BSA with CLSM (Confocal Laser Scanning Microscopy) [17]. Ye et al. grafted dual-functional block polymer brushes on TFC membrane as "defending" and "attacking" strategies against biofouling. Zwitterionic polymer brushes with strong

* Corresponding author.
E-mail address: ramong@technion.ac.il (G.Z. Ramon).

https://doi.org/10.1016/j.seppur.2019.02.045
Received 25 November 2018; Received in revised form 10 February 2019; Accepted 21 February 2019
Available online 23 February 2019
1383-5866/

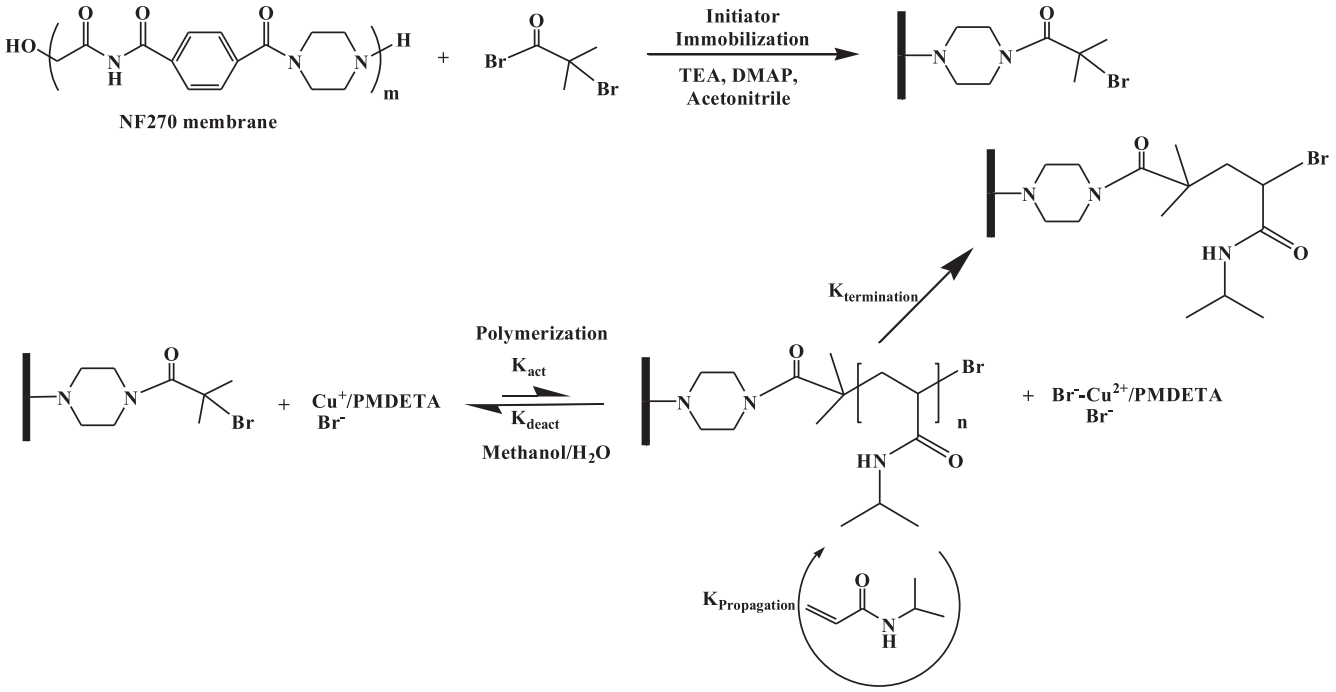

Fig. 1. Chemical reaction for grafting of PNIPAM polymer from the surface of NF270 membrane.

hydration capacity and quaternary ammonium salt (QAS) polymer brushes with bactericidal ability were sequentially grafted on TFC membranes via activators regenerated by electron transfer–atom transfer radical polymerization (ARGET-ATRP) [11]. In this study the anti-fouling properties were also tested by imaging adsorbed BSA. Imaging the fouled membrane at the end of an experiment or as a static experiment, has the disadvantage of missing important data about micro-scale processes such as deposition and release.

Unlike the majority of previous studies, we have investigated the use of surface modification using a responsive polymer. Responsive polymer brushes have been grafted from the membrane surface to actively suppress adsorption of foulnats [18–20]. One class of responsive polymer brushes are thermoresponsive polymers which, respond to changes in temperature and ionic strength [21]. Here, we have grafted poly N-isopropylacrylamide (PNIPAM) which exhibits a hydrophobic-hydrophilic phase transition at its lower critical solution temperature (LCST). We investigate colloidal deposition on modified, commercially-available thin-film composite (TFC) NF membranes with PNIPAM brushes. PNIPAM chains undergo swelling in aqueous solutions below the LCST. Above this temperature the polymer chains dehydrate and deswell. It has been found that salt ions tend to reduce the LCST of PNIPAM [22,23]. The effects of ions on the LCST follows the so-called Hofmeister series, which is the ability of ions to precipitate proteins from an aqueous solution. When adding salt to the PNIPAM solution, it creates competition between the amide O on the PNIPAM and the O (H_2O). The strong interactions between the divalent cations and water (electrostatic interaction) prevent them from forming direct contact interactions with the amide bond (dehydration process). The strong cation $-O(H_2O)$ interaction decreases the LCST due to salting-out effects [19].

A well-known method to investigate these micro-processes is through direct microscopic observation [24–29], a technique that provides a non-invasive, continuous, in-situ means to examine the deposition and release of particles during filtration using optical microscopy imaging techniques. Bernstein et al. modified low pressure RO membranes with different monomers to obtain negatively and positively charged and zwitterionic surfaces. In this study they used GFP-tagged bacteria and a fluorescent microscope to correlate between deposition and surface properties in a dynamic experiment [10].

Despite the mentioned research, there is still a lack of fundamental insight into the actual deposition kinetics and propensity of colloid adhesion onto brush-coated membranes. In the present study we use direct microscopic observation to investigate particle deposition on polymer-brush-coated, stimuli-responsive membranes.

2. Experimental

2.1. Materials

All chemicals used in this study are ACS reagent grade. Methanol (MeOH), and acetonitrile were purchased from EMD Millipore (Billerica, MA). Triethylamine (TEA), 4-dimethylaminopyridine (DMAP), N,N,N',N",N"-pentamethyl diethylenetriamine (PMDETA, 99%), copper (I) bromide, and copper (II) bromide (CuBr and $CuBr_2$, 99.999% trace metal basis) were procured from Sigma-Aldrich (Munich, Germany). 200 proof pure Ethanol (EtOH) was purchased from Koptec, VWR International (Radnor, PA). N-isopropylacrylamide (NIPAM, > 98%, stabilized with mequinol) was purchased from TCI America (Boston, MA). α-bromoisobutyryl bromide (BIB, 98%) was purchased from Alfa-Aesar (Ward Hill, MA). The deionized water used in the present investigation was obtained from a Thermo Fisher 18 MΩ Barnstead Smart2Pure system (Schwerte, Germany). Commercially available NF270 flat-sheet thin film composite polyamide membranes were obtained from Dow Filmtec (Edina, Minnesota). All membrane samples used in this study were cut from large sheets into circular specimen with a diameter of 25 mm.

2.2. Membrane modification

Membrane modification was performed in 2 steps, beginning with immobilization of the initiator on the membrane and followed by controlled growth of the polymer from the initiator on the membrane by ATRP (see Fig. 1 for schematic illustration).

Immobilization of initiator to membrane. Before use, the membranes were washed in 1:1(v/v) EtOH/water solution for 2 h and dried overnight in vacuum oven at 40 °C. Acetonitrile was used as the main

solvent which was dried over activated molecular sieves prior to its use.

The initiator immobilization solution was prepared by dissolving 100 mM TEA, 5 mM DMAP in 20 ml dry acetonitrile. The dried NF270 membrane was transferred to the immobilization solution. Finally, 1% by volume of the initiator, BiB, was then added to the main solution then quickly sealed to avoid moisture. The reaction conditions were 15 min at room temperature. After 15 min, the reaction was quenched with water. The membrane was washed in a 1:1(v/v) EtOH/water mixture, 3 times for 3 h, and then dried in vacuum oven at 40 °C overnight.

Atom transfer radical polymerization. Following initiator immobilization, membrane modification with NIPAM was conducted by atom transfer radical polymerization reaction (ATRP). Each membrane disc was placed in a flask, then evacuated and backfilled with argon at least three times.

The main solution was then prepared by mixing NIPAM:CuBr:PMDETA at 100:1:3 M ratio in a water/methanol mixture (9:1, v/v). First NIPAM was added to the water/MeOH mixture and purged with argon and agitated for at least 30 min. Subsequently, PMDETA was added into solution under argon with continuous stirring for 15 min. Next, CuBr was added to the reaction flask while mixing and degassing with argon for another 15 min. Finally, the reaction solution was cannulated into a sealed argon filled flask which contained the membrane.

The reaction flask had to be sealed carefully in order to prevent oxidization during reaction. The reaction flask was incubated at room temperature for one hour. Thereafter, the solution was removed from the flask, and thoroughly washed with a mixture of water/methanol 1:1 (v/v) at least 3 times, then with a mixture of water/ethanol 1:1 (v/v) again 3 times for 3 h. Modified membranes were stored in mixture water/ethanol 1:1 (v/v).

2.3. Membrane characterization

Atomic force microscopy. After vacuum drying at 40 °C, surface topography of the modified NF270 membrane was measured by using an atomic force microscopy (AFM) equipped with Dimension Icon AFM from Bruker, Santa Barbara, CA. Nanoscope V815R3sr1 program was used to run the AFM measurement and NanoScope Analysis program was used to analyze the results. The reliable automatic image operation technology, ScanAsyst mode, was used to image the topography of membranes at room temperature in air using an etched silicon tip on a nitride lever which is coated with a 100 nm aluminum layer. The nominal spring constant of the cantilever used was 0.4 N/m and 70 kHz respectively. A standard scan rate of 1 Hz with 512 samples per line was used for imaging the membrane sections. The measured heights of the images were then flattened in order to obtain the final images. AFM imaging was conducted at ~20 °C, below the LCST of the grafted PNIPAM brushes.

Attenuated Total Reflectance Fourier-Transform Infrared Spectroscopy (ATR-FTIR). ATR-FTIR spectroscopy provides qualitative information about functional groups at the top of the membrane. Fourier-transform infrared (FT-IR) spectra were acquired using a Shimadzu IRAffinity-1 equipped with a PIKE single-reflection horizontal ATR accessory. ATR-FTIR spectra was averaged over 1000 scans covering a range of 600–4000 cm^{-1}. Prior to analysis, membranes were dried overnight in a vacuum oven at 40 °C.

X-ray Photoelectron Spectroscopy (XPS). Compared to ATR-FTIR, XPS is far more surface sensitive. XPS typically detects elements in the top 10 nm from the membrane surface, and can provide information on the elemental composition present on the membrane surfaces. A Versa Probe Station Physical Electron 5800 ultrahigh vacuum XPS-Auger spectrometer (PHI) (Chanhassen, MN, USA) at a 45° takeoff angle was used in this study. For each sample, 50 scans with 3 repetitions at high resolution of 0.1 eV step-change, focusing on the Br regions, were averaged to characterize small changes in the surface chemistry upon grafting.

Contact angle. Static contact angles for all membranes were measured using the captive bubble method at room temperature and pressure (OCA 20, Future Digital Scientific Corp., Garden City, NY, USA). Membranes were cut into small pieces and pasted on a metal chip with double sided tape. The metal chip was then placed on the top of a transparent container with the active surface of the membrane facing down. The container was filled with DI water and placed in front of the camera which is able to capture the air bubble. An air bubble (2 µl) was injected into the water solution, allowed to attach to the membrane surface and then the image was recorded by a camera. By using the circle fitting method, the angle made between the air bubble and the membrane surface was measured every 0.1 s. Data was collected for the first 3 s at 5 different locations. The average of these 150 measurements yield the final result.

Zeta potential. The zeta potential of the membranes was measured with a Delsa Nano HC particle analyzer manufactured by Beckman Coulter (Brea, CA). The main solution was prepared by mixing 200 µl of zeta potential standard solution for flat surface from Beckman Coulter in 25 ml of 10 mM sodium chloride. The pH was adjusted using 10 mM sodium hydroxide and 10 mM hydrochloric acid. Each data point was an average of 3 replications.

2.4. Colloidal deposition experiments

Feed solution for deposition experiments. The feed stream contained Deionized (DI) water supplied by a Milli-Q ultrapure water device, 0.01 M sodium chloride (ACS reagent grade, Sigma-Aldrich, St. Louis, MO, USA) as a background electrolyte and fluorescent beads as model foulants: Carboxyl-modified 1 µm diameter polystyrene beads (FluoSpheres, Life Technologies, (Invitrogen, Ltd.), Paisley, UK) and amine-modified 1 µm diameter polystyrene beads (Sigma-Aldrich, St. Louis, MO, USA). The carboxyl-functionalized particles emit orange fluorescence at 560 nm (excitation at 540 nm), amine-functionalized particles emit yellow-green fluorescence at 505 (excitation at 470 nm). The solution provided by the manufacturer contained $4.5{\cdot}10^{10}$ [10] particles/ml (2% solids) and was first diluted to 10^8 particles/ml, to avoid contamination, and then diluted again to a fixed concentration of 10^6 particles/ml, used in the experiments.

Experimental system. The experimental setup is shown schematically in Fig. 2. A custom-made crossflow filtration cell, with a sapphire glass viewing port, allows in-situ observation using a confocal laser scanning microscope (TCS SP8, Leica Microsystems, Wetzler, Germany). Channel dimensions within the cell are 0.6 mm (H), 6 mm (W), 36 mm (L) with a total membrane filtration area of 216 mm^2. The flow cell was mounted on the microscope stage equipped with a 25×, water immersion objective, corresponding to a field of view of 262,144 pixels (≈384,400 μm^2).

Experiments were carried out at room temperature (22 °C) and pH 6 (unadjusted). The feed vessel was placed on top of a magnetic plate and the solution was stirred at 400 rpm. The applied feed pressure was set to 3 bar, using compressed nitrogen connected to the feed vessel. A programmable gear pump (Micropump, Cole Parmer, Vernon Hills, IL, USA) was used to maintain a constant cross-flow velocity of 0.07 m/s and recirculated the retentate back to the feed vessel. The permeate outlet was connected to a syringe pump, set at a constant flow rate, to ensure a constant flux through the membrane. Changes of the transmembrane pressure (TMP), occurring during the experiment due to fouling, were monitored by a differential pressure transducer (PX409, omega engineering, UK). Electrical conductivity and temperature were measured continuously with a probe (M200 easy line, Mettler Toledo, USA) dipped into the feed vessel. Electrical conductivity of the permeate was measured at the end of each experiment by a probe (cyerscan PC 300, Eutech instruments, Singapore).

Deposition and cleaning experiments. Initially, air bubbles were removed, and the membrane compacted before each experiment. The

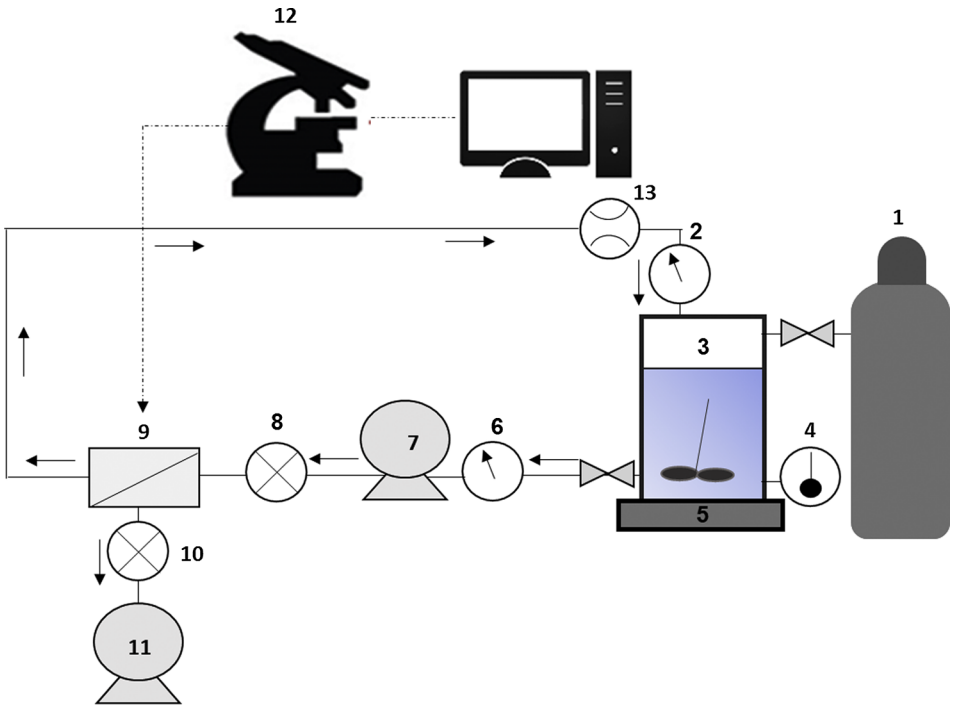

Fig. 2. A schematic drawing of the experimental system: 1 – Pressurized gas tank, 2 – Pressure gauge, 3 – Pressurized feed vessel, 4 – Conductivity probe & thermometer, 5 – Magnetic stir plate, 6 – Pressure gauge, 7 – Gear pump, 8 – Pressure indicator, 9 – Flow cell, 10 – Pressure indicator, 11 – syringe pump, 12 – confocal microscope and computer, 13 – Rotameter.

Table 1
Measured physicochemical properties of membranes.

			Base NF270	PNIPAM
Water permeability	L_p	(m/s·bar)	$5.5 \cdot 10^{-6}$	$1.5 \cdot 10^{-6}$
Salt rejection[a]	R	(%)	70	95
Zeta potential[b]	ζ	(mV)	−11.2	−4.5
Contact angle	θ	(°)	18.5	55.1
Surface roughness[c]	RMS	(nm)	R_q = 4.34 R_a = 3.42	R_q = 7.65 R_a = 6.20

[a] Measured for solution containing 0.01 M NaCl.
[b] Measured in 0.01 M NaCl solution at pH 6.
[c] Scanning size 2 μm × 2 μm.

feed solution was pumped into the flow cell for 40 min for deposition, during which five random images of the membrane surface at different locations were acquired every 5 min. Deposition was followed by a *cleaning* protocol composed of 5 steps. First, the feed pressure was reduced to zero (designated as *TMP = 0*) to eliminate permeation. Then the feed solution was replaced with a concentrated salt solution containing 1.5 M NaCl (*salt*), after which the feed was replaced by MilliQ water (*water*). The last two steps were repeated twice. Each of the cleaning steps lasted 20 min. After the 'cleaning cycles' were completed, the flux recovery was determined with DI water.

The average permeation rate at a pressure of 3 bar is 17.7 μm/s and 3.6 μm/s for NF270 and PNIPAM-coated NF270, respectively. To overcome this difference in conditions, experiments were performed under two different conditions – *long-term deposition* at the same water flux (5.5 μm/s) and particle flux and a *deposition-release protocol* (deposition stage followed by the cleaning protocol outlined above), with a fixed particle flux towards the membrane. In the latter case, to maintain a similar particle flux (or a larger particle flux for PNIPAM, so as to be conservative), the particle concentration in the PNIPAM experiments was 5 times higher than that for the base NF270. The particle flux towards the membrane was $\approx 2 \cdot 10^{-5}$ (particle #/μm^2·s) and was calculated using

$$J_s = J_w C_s \quad (1)$$

where J_s is the particle flux towards the membrane (#/s·μm^2), C_s is the particle concentration (#/μm^3) and J_w is the water flux trough the membrane (μm/s).

Image Acquisition and Analysis. The high-resolution images acquired through the microscope were exported to a PC and analyzed with MATLAB (version R2016a). Each image was represented in pixels by modifying it to 8-bit integers. In a raw gray-scale image, each pixel holds 256 steps of gray level values which describes the intensity of the light (0 = black, 255 = white). Fluorescent microbeads appeared white against the dark membrane background. Then, a threshold was chosen to eliminate background noise in the images. The converted black and white images were used to determine the fractional coverage by particles at a given time through individual pixel enumeration.

3. Results and discussion

3.1. Membrane characterization

Surface characteristics of base NF270 and PNIPAM-grafted NF270 membranes are presented in Table 1. The water permeability and salt rejection of the base NF270 and PNIPAM-modified membranes were measured using a dead-end cell at a range of applied hydraulic pressures. As indicated by other studies, the grafted nanostructure causes a reduction in average membrane permeability [20,21]. Compared to the base NF270, PNIPAM-grafted membranes exhibited a higher contact angle (CA) (Table 1). The surface of NF270 is known to be quite hydrophilic, as indicated by low CA values (18.5°) measured, a value in good agreement with other reports [7,13]. The increased CA upon PNIPAM modification (55.1°) is due to the higher hydrophobicity of the PNIPAM chains. Zeta potential (Table 1) provides a measure of the effective surface charge. Both membranes exhibit a negative charge at pH 6 (experimental conditions), but the value is 2.5 times larger for the NF270 base membrane, presumably since PNIPAM chains create partial screening of the base membrane surface charge.

Fig. 3(a) shows the ATR-FTIR spectra of base NF270 and membrane grafted with PNIPAM. Changes in the ATR–FTIR spectra after modification confirmed that the functional PNIPAM brushes have been grafted from the dense layer of TFC membrane (NF270). Grafted PNIPAM brushes are identified by additional bands at ~1660 and ~1540 cm^{-1} for C═O and N−H stretching, respectively. Polysulfone,

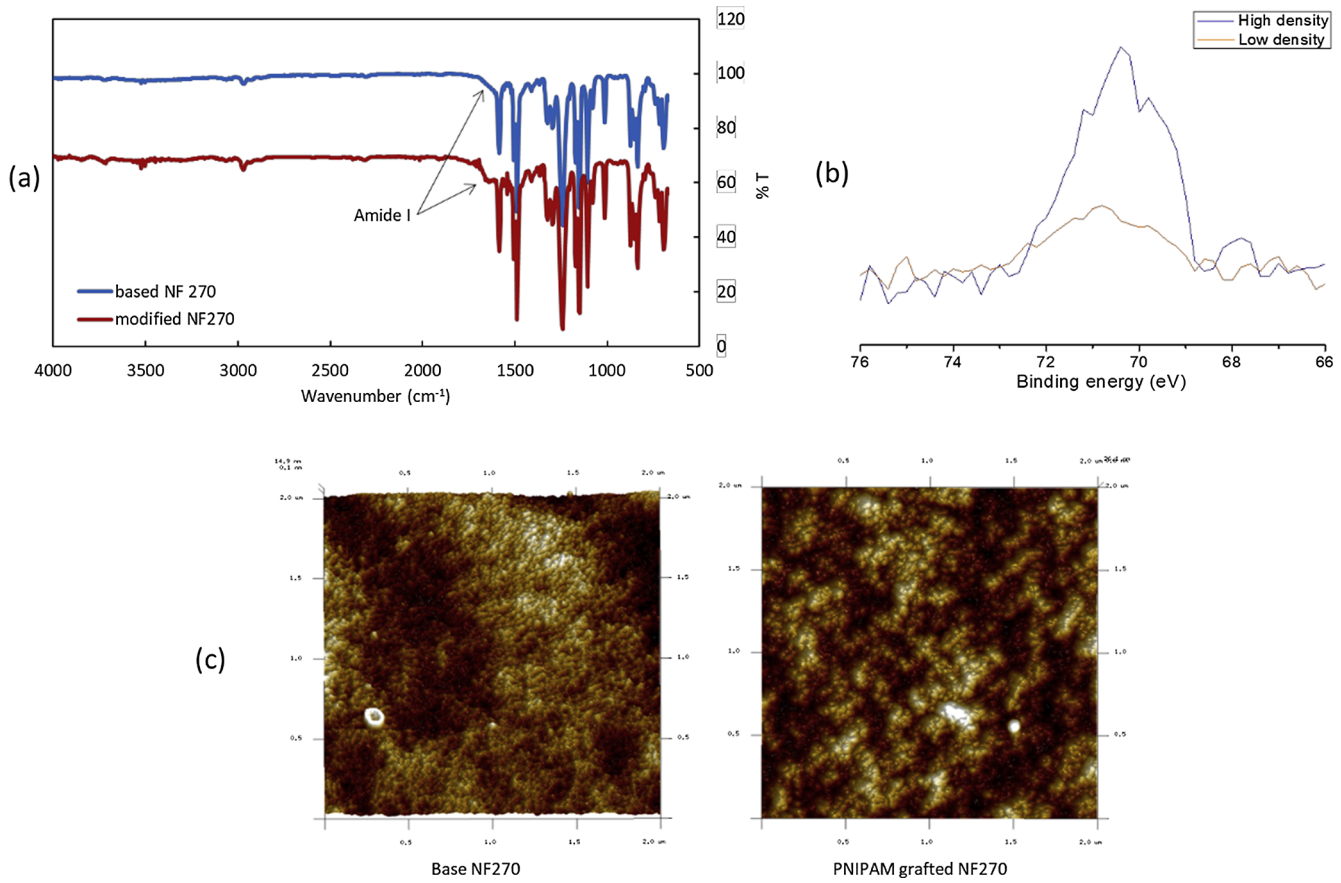

Fig. 3. (a) ATR FTIR spectra for unmodified NF270 membrane (blue) and PNIPAM modified-NF270 membrane (red). (b) Bromine peak for modified membranes. (c) AFM images of unmodified NF270 membrane and PNIPAM modified-NF270 membrane. (For interpretation of the references to colour in this figure legend, the reader is referred to the web version of this article.)

material of the porous support, has a strong 1585 cm^{-1} band and a double band at ~1500 cm^{-1} assigned to aromatic ring stretching, a result very close to other reports [20,29]. Fig. 3(b) presents high resolution XPS data exhibiting a Br peak after ATRP for low and high density of PNIPAM.

The AFM images for base NF270 and PNIPAM-grafted NF270 membranes are presented in Fig. 3(c). A significant difference in surface morphologies between the base and grafted membrane surfaces is observed. The surface morphology of the unmodified NF270 membrane is smoother than the modified membrane. This difference is also reflected in their root mean square (RMS) surface roughness values (Table 1). The unmodified membrane exhibits RMS surface roughness of 3.4 nm in the scan area of 2 × 2 μm, significantly lower than for the grafted membrane surface (6.2 nm).

3.2. Membrane performance

PNIPAM chains undergo a hydrophilic-hydrophobic phase transition above-below their LCST (~30 °C), i.e. above this temperature the chains will change their conformation from hydrated to dehydrated and collapsed conformation in DI water. Fig. 4(a) gives results for molecular dynamics (MD) simulations. The degree of polymerization for the computational experiments was 50.

One way to evaluate this phase transition is by measuring the permeate flux. Grafting reaction conditions were chosen in order to minimize the decrease in flux due to the grafted nanostructure while ensuring the change in conformation of the polymer chains could be detected. In the absence of thermo-responsive chains, as the temperature is increased, the permeate flux is expected to increase due to decreasing viscosity. However, in the presence of PNIPAM chains, the flux behaves in the opposite way as we have indicated in our earlier studies. Above the LCST, the chains dehydrate and adopt a collapsed conformation. This has the effect of increasing the resistance to permeate flow through the grafted nanolayer [17]. Fig. 4(b) presents the ratio between the permeate flux measured for heated water to room temperature water as a function of the heated solution temperature, for a PNIPAM grafted membrane. The flux decreases up to 40% from its initial value, as the temperature reaches 50°C. This observed trend is considered to be evidence of the phase transition. It is known that the presence of salt ions in the solution affects the LCST of PNIPAM chains, as the strong interactions between the salt cations and water prevent them from forming direct contact interactions with the amide bond, so that the chains undergo dehydration and collapse at room temperature (~22 °C).

3.3. Deposition experiments

PNIPAM brushes appear to impart antifouling properties to surfaces based on earlier studies [20,30,31]. To quantify how the grafting of PNIPAM brushes changed the fouling propensity of the membrane, we used a direct observation technique to measure surface coverage during deposition and after cleaning.

Particles deposition. Microscopic images of carboxyl-modified polystyrene bead deposition are presented in Fig. 5(b). Red dots represent the particles deposited on the membrane. After 30 min of dead-end filtration, only 2% of the PNIPAM surface is covered, while the ungrafted membrane coverage is 12%. Fig. 5(a) shows the surface coverage of carboxylate-modified polystyrene beads under different flow regimes: dead-end filtration, 0.02 m/s cross flow, 0.05 m/s cross flow and 0.07 m/s cross flow. While surface coverage on PNIPAM-modified

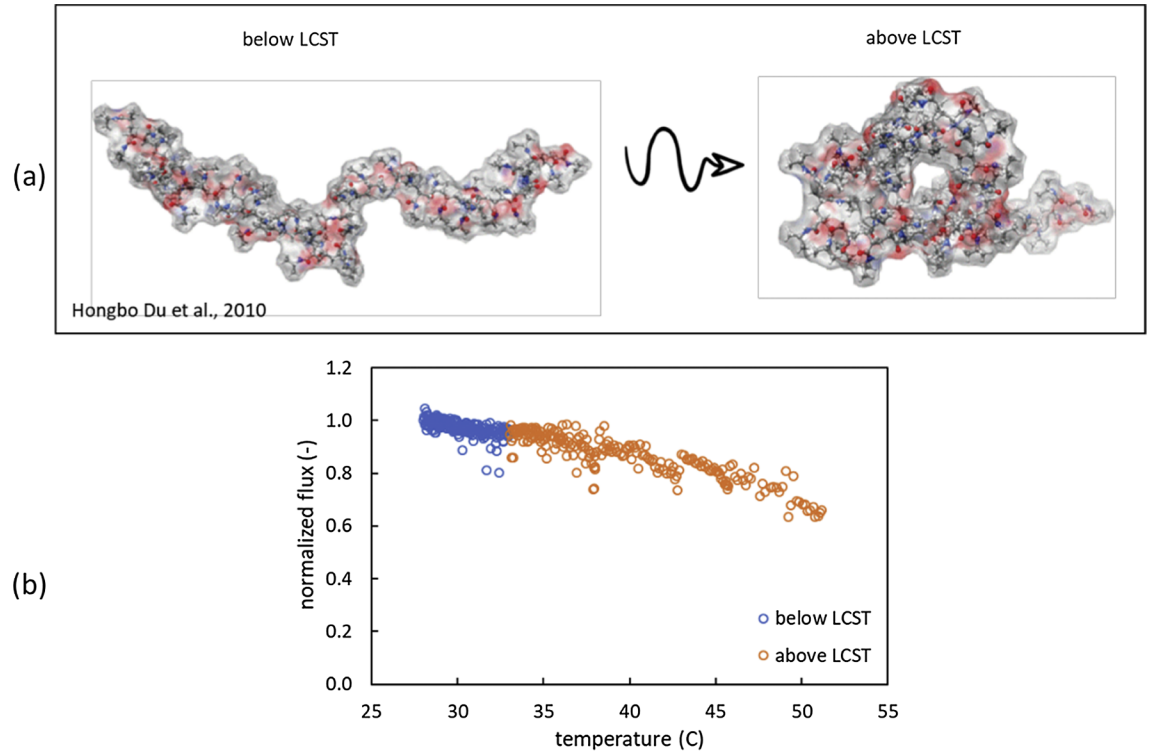

Fig. 4. (a) 3D MD simulation of PNIPAM phase transition [19] (b) the ratio between PNIPAM flux above LCST and below LCST.

membrane remians under 5% after 60 min, the base NF270 reaches 15% coverage in half the time. It is clear that the grafted chains prevent the particles from reaching the membrane surface. Fig. 5(c) shows the measured surface coverage of the membrane under the same flow conditions (permeate flux and cross flow velocity) and solution chemistry. This time, deposition lasted for a relatively long period of time (100 min). For every time point measured, the NF270 base membrane coverage is greater than that of PNIPAM-grafted membrane. Hence, NF270 membrane is more prone to adhesion of particles than the PNIPAM-modified membrane.

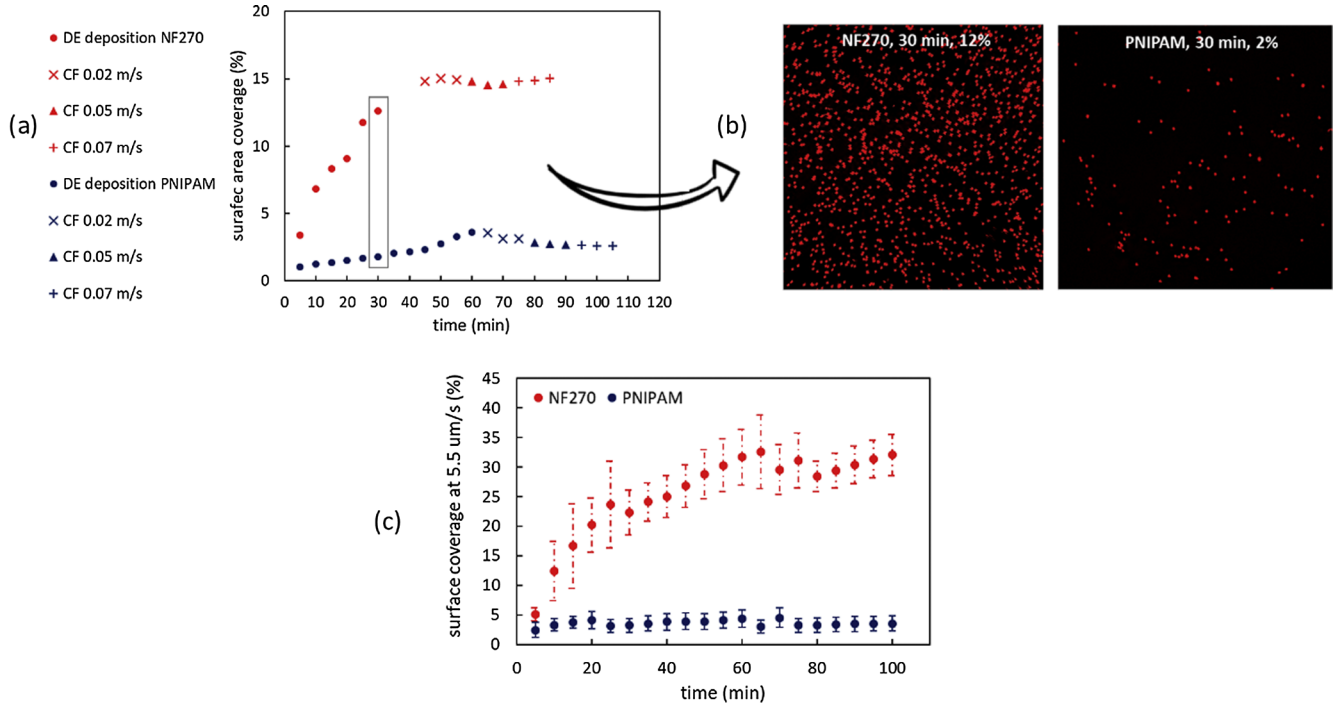

Fig. 5. (a) NF270 (red) and PNIPAM (blue) surface coverage by polystyrene beads at 4 flow conditions: DE-deposition at dead end, CF – cross flow of 3 velocities: 0.02, 0.05 & 0.07 m/s; (b) microscopic images of surface area covered by polystyrene beads after 30 min of dead end deposition; (c) NF270 (red) and PNIPAM (blue) surface coverage by polystyrene beads at the same permeation flux 5.5 μm/s and particle flux $\sim 3 \cdot 10^{-5}$ #/s·μm^2. (For interpretation of the references to colour in this figure legend, the reader is referred to the web version of this article.)

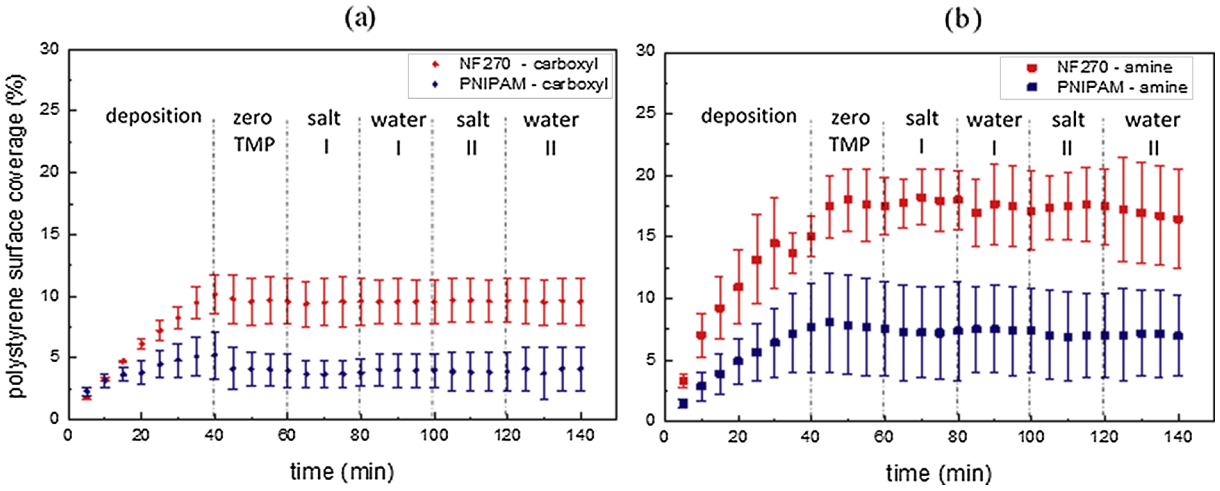

Fig. 6. Mean surface area covered by (a) carboxyl-polystyrene beads and (b) amine-polystyrene beads, plotted against time for NF270 (red dots) and PNIPAM (blue dots). Ionic strength 0.01 M, cross flow velocity 0.07 m/s, carboxyl-particle flux: NF270 $2.2 \cdot 10^{-5}$ #/s·μm^2, PNIPAM $2.7 \cdot 10^{-5}$ #/s·μm^2; amine-particle flux: NF270 $1.5 \cdot 10^{-5}$ #/s·μm^2, PNIPAM $2.7 \cdot 10^{-5}$ #/s·μm^2. (For interpretation of the references to colour in this figure legend, the reader is referred to the web version of this article.)

Particles charge, deposition and kinetics. As deposition is affected by charge interactions, two oppositely charged particles were tested – negative carboxyl-modified particles (at pH 6 with zeta potential is −28 mV) and slightly positively charged amine-modified particles (at pH 6 zeta potential is 4 mV).

Fig. 6(a) & (b) shows the averaged membrane surface coverage of polystyrene particles counted at the same location in the course of deposition at different times (5–40 min). The enhanced deposition of amine-modified particles, compared to carboxyl-modified particles, is attributed to electrostatic attraction between the particles and the membrane. For the flow conditions used, deposition follows first-order kinetics with a linear trend corresponding to R^2-values of 0.993, 0.968, 0.975 and 0.972 for carboxyl-NF270, carboxyl-PNIPAM, amine-NF270 and PNIPAM-amine, respectively (calculated for the first 30 min of deposition). The linear slope of fractional surface coverage, $\Delta\theta(t)$, plotted against time, t, gives the net surface coverage rate constant, k_{sc} (Table 2). The rate constant calculated for the base NF270 membrane is 2.6 times larger than for the PNIPAM-modified membrane for the carboxyl particles and 3.6 times larger for the amine particles. The values presented emphasize the fast kinetics of particles deposition on the NF270 base membrane. Moreover, as expected, amine-particles deposit faster than carboxyl particles. Since both membranes are negatively charged at this pH, it is reasonable to assume that repulsive electrostatic forces influence the deposition kinetics.

Cleaning cycles. The membrane surface coverage is plotted against time in Fig. 6(a) for carboxyl-modified particles and Fig. 6(b) for amine-modified particles. As particles move toward the membrane surface, they reach the point at which they may touch the PNIPAM chains. Since the particles are affected by the viscous 'permeation drag' force, they are drawn closer to the surface [32,33]. In the presence of PNIPAM, the particles compress the chains to the point where the repulsive force of the brush equals the permeation drag. Brush compression can influence the 'cleaning' mechanism, as it is assumed to also potentially affect the reversibility of particle deposition. As seen in Fig. 6(a), the mean coverage at the first point after deposition (t = 45 min) is lower than the one before it. For the NF270, 4% of the particles were detached and for PNIPAM 21% of them were detached. When the pressure is shut-off, the system experiences a great change (relaxation) in the force balance keeping the particles deposited at a certain position above the membrane. Particles that were held close to the membrane, primarily by permeation, are now released. The severity of this release is greater for the PNIPAM, since the brush layer acts to separate the particles from the surface. For the positively charged amine-particles in Fig. 6(b), the opposite trend can be observed. Since the 'particle-membrane' system is now composed of two opposite charges, the significance of the charge in the force balance is greater. A striking feature of these experiments is the fact that particle deposition was mostly irreversible for both membranes, particularly the unmodified membrane. The cleaning cycles do not seem to be as effective as hypothesized, since there is no significant change in surface coverage during the cycles, for both membranes. Possibly, deposition occurs at 'defect' sites, thus brush 'activation' cannot release the foulants. It may also be that adhesion, once occured, is stronger than the energy of brush collapse and expansion.

Table 2
Surface coverage rate constant ksc (min-1) for polystyrene particles.

	Carboxyl-particles		Amine-particles	
	k_{sc} (min^{-1})	Coverage[a] (%)	k_{sc} (min^{-1})	Coverage[a] (%)
NF270	0.0026	10	0.0043	18
PNIPAM	0.0010	5	0.0012	8

[a] Membrane surface coverage after 30 min of deposition.

In this study we have investigated adsorption/desorption of polystyrene spheres under carefully controlled conditions. As expected, the level of adsorption depends on the sum of the attractive forces between the membrane surface and polystyrene spheres. The presence of flexible polymer brushes at the membrane surface provides an additional kinetic barrier to adsorption probably due to the potential loss of entropy of the adsorbed species, polymer brushes and associated water molecules. Release of the adsorbed species is more complex than previously described. Adsorption onto the PNIPAM brushes could affect the ability of the PNIPAM brushes to switch between a hydrated and dehydrated conformation below and above the LCST. This in turn may limit the possibility of releasing adsorbed foulants. Consequently, adsorption of foulants may limit the reversibility of switching conformation above and below the LCST. In addition, it is likely that deformable particles such as oil droplets may behave very differently to rigid polystyrene spheres.

4. Conclusions

Direct microscopic observation of colloidal deposition on PNIPAM-brush-coated NF membranes offers new insights into anti-fouling properties of brush-coated membranes, since very little direct evidence

exists on such systems. Polystyrene particles were used to foul NF270 and PNIPAM-modified NF270 membranes. Flux measurements of the PNIPAM-modified NF270 membranes demonstrated reversible conformational changes of the brushes. Cross-flow filtration experiments performed under confocal microscopy indicate that the brush layer significantly decreases particle deposition, presumably by preventing them from approaching the membrane surface by steric repulsion. Particle deposition onto PNIPAM-modified membranes was consistently lower, regardless of the particles surface charge. Despite the success in decreasing deposition, the suggested cleaning protocol had little effect, as deposition proved to be mostly irreversible. Here, the degree of reversibility was lower for the unmodified membrane, suggesting that some deposited particles only weakly interacted with the brush-coated membrane. While this work provides much needed, direct evidence of the anti-fouling properties of brush coated membranes, clearly there is a need to test other, potentially better performing systems.

Acknowledgments

This research was funded by the US-Israel Binational Agricultural R &D fund (BARD) award IS-4768-14R.

References

[1] M.M. Pendergast, E.M.V. Hoek, A review of water treatment membrane nanotechnologies, Energy Environ. Sci. 4 (2011) 1946.
[2] M. Elimelech, W.a. Phillip, The future of seawater desalination: energy, technology, and the environment, Science 333 (2011) 712–717.
[3] R. Semiat, Energy issues in desalination processes, Environ. Sci. Technol. 42 (2008) 8193–8201.
[4] M.A. Shannon, et al., Science and technology for water purification in the coming decades, Nature 452 (2008) 301–310.
[5] E.M. Vrijenhoek, S. Hong, M. Elimelech, Influence of membrane surface properties on initial rate of colloidal fouling of reverse osmosis and nanofiltration membranes, J. Memb. Sci. 188 (2001) 115–128.
[6] W. Guo, H.-H. Ngo, J. Li, A mini-review on membrane fouling, Bioresour. Technol. 122 (2012) 27–34.
[7] N. Park, B. Kwon, S.D. Kim, J. Cho, Characterizations of the colloidal and microbial organic matters with respect to membrane foulants, J. Memb. Sci. 275 (2006) 29–36.
[8] D. He, H. Susanto, M. Ulbricht, Photo-irradiation for preparation, modification and stimulation of polymeric membranes, Prog. Polym. Sci. 34 (2009) 62–98.
[9] A. Al-Amoudi, R.W. Lovitt, Fouling strategies and the cleaning system of NF membranes and factors affecting cleaning efficiency, J. Memb. Sci. 303 (2007) 4–28.
[10] R. Bernstein, S. Belfer, V. Freger, Bacterial attachment to RO membranes surface-modified by concentration-polarization-enhanced graft polymerization, Environ. Sci. Technol. 45 (2011) 5973–5980.
[11] G. Ye, J. Lee, F. Perreault, M. Elimelech, Controlled architecture of dual-functional block copolymer brushes on thin-film composite membranes for integrated 'defending' and 'attacking' strategies against biofouling, ACS Appl. Mater. Interfaces 7 (2015) 23069–23079.
[12] S. Zhou, et al., Fabrication of temperature-responsive ZrO2 tubular membranes, grafted with poly (N-isopropylacrylamide) brush chains, for protein removal and easy cleaning, J. Memb. Sci. 450 (2014) 351–361.
[13] A. Ben-David, et al., Facile surface modification of nanofiltration membranes to target the removal of endocrine-disrupting compounds, J. Memb. Sci. 357 (2010) 152–159.
[14] S. Mondal, S.R. Wickramasinghe, Photo-induced graft polymerization of N-isopropyl acrylamide on thin film composite membrane: produced water treatment and antifouling properties, Sep. Purif. Technol. 90 (2012) 231–238.
[15] D. Wandera, H.H. Himstedt, M. Marroquin, S.R. Wickramasinghe, S.M. Husson, Modification of ultrafiltration membranes with block copolymer nanolayers for produced water treatment: the roles of polymer chain density and polymerization time on performance, J. Memb. Sci. 403–404 (2012) 250–260.
[16] H.Y. Yu, Y. Kang, Y. Liu, B. Mi, Grafting polyzwitterions onto polyamide by click chemistry and nucleophilic substitution on nitrogen: a novel approach to enhance membrane fouling resistance, J. Memb. Sci. 449 (2014) 50–57.
[17] Z. Liu, et al., Modification of thin film composite polyamide membranes with 3D hyperbranched polyglycerol for simultaneous improvement in their filtration performance and antifouling properties, J. Mater. Chem. A 5 (2017) 23190–23197.
[18] G. Song, A. Sengupta, X. Qian, S.R. Wickramasinghe, Investigation on suppression of fouling by magnetically responsive nanofiltration membranes, Sep. Purif. Technol. 205 (2018) 94–104.
[19] H.H. Himstedt, A. Sengupta, X. Qian, S.R. Wickramasinghe, Magnetically responsive nano filtration membranes for treatment of coal bed methane produced water, J. Taiwan Inst. Chem. Eng. (2018) 1–12.
[20] S. Darvishmanesh, X. Qian, S.R. Wickramasinghe, Responsive membranes for advanced separations, Curr. Opin. Chem. Eng. 8 (2015) 98–104.
[21] X. Qian, Q. Yang, A. Vu, S.R. Wickramasinghe, Localized heat generation from magnetically responsive membranes, Ind. Eng. Chem. Res. 55 (2016) 9015–9027.
[22] H. Du, S.R. Wickramasinghe, X. Qian, Specificity in cationic interaction with poly (N-isopropylacrylamide), J. Phys. Chem. B 117 (2013) 5090–5101.
[23] H. Du, R. Wickramasinghe, X. Qian, Effects of salt on the lower critical solution temperature of poly (N-isopropylacrylamide), J. Phys. Chem. B 114 (2010) 16594–16604.
[24] A. Subramani, E. Hoek, Direct observation of initial microbial deposition onto reverse osmosis and nanofiltration membranes, J. Memb. Sci. 319 (2008) 111–125.
[25] S. Wang, G. Guillen, E.M.V. Hoek, Direct observation of microbial adhesion to membranes, Environ. Sci. Technol. 39 (2005) 6461–6469.
[26] H. Li, A.G. Fane, H.G.L. Coster, S. Vigneswaran, Direct observation of particle deposition on the membrane surface during crossflow microfiltration, J. Memb. Sci. 149 (1998) 83–97.
[27] A. Subramani, X. Huang, E.M.V. Hoek, Direct observation of bacterial deposition onto clean and organic-fouled polyamide membranes, J. Colloid Interface Sci. 336 (2009) 13–20.
[28] G. Fux, G.Z. Ramon, Microscale dynamics of oil droplets at a membrane surface: deformation, reversibility, and implications for fouling, Environ. Sci. Technol. 51 (2017) 13842–13849.
[29] S. Kang, A. Subramani, E.M.V. Hoek, M.A. Deshusses, M.R. Matsumoto, Direct observation of biofouling in cross-flow microfiltration : mechanisms of deposition and release, J. Memb. Sci. 244 (2004) 151–165.
[30] C.-C. Hsu, C.-S. Wu, Y.-L. Liu, Multiple stimuli-responsive poly(vinylidene fluoride) (PVDF) membrane exhibiting high efficiency of membrane clean in protein separation, J. Memb. Sci. 450 (2014) 257–264.
[31] N. Tomer, S. Mondal, D. Wandera, S.R. Wickramasinghe, S.M. Husson, Modification of nanofiltration membranes by surface-initiated atom transfer radical polymerization for produced water filtration, Sep. Sci. Technol. 44 (2009) 3346–3368.
[32] G.Z. Ramon, H.E. Huppert, J.R. Lister, H.A. Stone, On the hydrodynamic interaction between a particle and a permeable surface, Phys. Fluids 25 (2013).
[33] G.Z. Ramon, E.M.V. Hoek, On the enhanced drag force induced by permeation through a filtration membrane, J. Memb. Sci. 392–393 (2012) 1–8.